JACS
JOURNAL OF THE AMERICAN CHEMICAL SOCIETY
Article
pubs.acs.org/JACS

Low-Temperature Processed Ga-Doped ZnO Coatings from Colloidal Inks

Enrico Della Gaspera,[†,⊥] Marco Bersani,[†] Michela Cittadini,[†] Massimo Guglielmi,[†] Diego Pagani,[‡] Rodrigo Noriega,[§] Saahil Mehra,[∥] Alberto Salleo,[∥] and Alessandro Martucci*[,†]

[†]Dipartimento di Ingegneria Industriale, Università di Padova, Via Marzolo, 9, 35131 Padova, Italy

[‡]Fondazione Salvatore Maugeri−IRCCS Centro di Ricerche Ambientali, Via Svizzera, 16, 35127 Padova, Italy

[§]Department of Applied Physics and [∥]Department of Materials Science & Engineering, Stanford University, Stanford, California 94305, United States

Supporting Information

ABSTRACT: We present a new colloidal synthesis of gallium-doped zinc oxide nanocrystals that are transparent in the visible and absorb in the near-infrared. Thermal decomposition of zinc stearate and gallium nitrate after hot injection of the precursors in a mixture of organic amines leads to nanocrystals with tunable properties according to gallium amount. Substitutional Ga^{3+} ions trigger a plasmonic resonance in the infrared region resulting from an increase in the free electrons concentration. These nanocrystals can be deposited by spin coating, drop casting, and spray coating resulting in homogeneous and high-quality thin films. The optical transmission of the Ga−ZnO nanoparticle assemblies in the visible is greater than 90%, and at the same time, the near-infrared absorption of the nanocrystals is maintained in the films as well. Several strategies to improve the films electrical and optical properties have been presented, such as UV treatments to remove the organic compounds responsible for the observed interparticle resistance and reducing atmosphere treatments on both colloidal solutions and thin films to increase the free carriers concentration, enhancing electrical conductivity and infrared absorption. The electrical resistance of the nanoparticle assemblies is about 30 kΩ/sq for the as-deposited, UV-exposed films, and it drops down to 300 Ω/sq after annealing in forming gas at 450 °C, comparable with state of the art tin-doped indium oxide coatings deposited from nanocrystal inks.

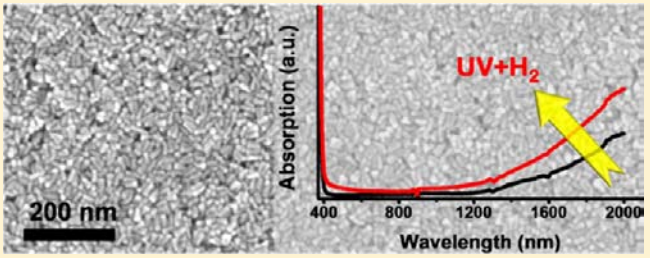

1. INTRODUCTION

Transparent conducting oxide (TCO) coatings are fundamental components in many applications where high transmission in the visible, absorption/reflection in the near-infrared (NIR), and high electrical conductivity are required. At present, the dominant markets for TCO applications are energy-efficient windows, flat panel displays, and the photovoltaic industry.[1] For these purposes, the most widely used TCOs are tin-doped indium oxide (ITO), fluorine-doped tin oxide (FTO), antimony-doped tin oxide (ATO), aluminum-doped zinc oxide (AZO), gallium-doped zinc oxide (GZO), and indium-doped zinc oxide (IZO).[2] These coatings are typically deposited using costly processes, such as chemical vapor deposition (CVD) and physical vapor deposition (PVD).[3]

The realization of nanocrystal (NC) inks based on TCO colloids dispersed in proper solvents would be of great advantage for many applications, because the related wet-deposition techniques like spraying, inkjet/gravure printing, and spinning allow for the coating of a broad choice of substrate materials and shapes at reasonable cost.[4] Moreover, the synthesis of NC TCO inks allows also for the deposition at low temperature on plastic substrates, which are known to be temperature sensitive. There has been recently a great effort in the preparation of a variety of materials such as silver nanowires,[5] ZnO nanoparticles,[6] and carbon nanotubes[7] for directly printable electronics from solutions of active inks. Syntheses of colloidal ITO,[8−10] ATO,[11] and AZO[12] have been recently reported. A GZO NC synthesis has been published recently as well,[13] but the as-synthesized nanoparticles are extremely aggregated resulting in milky suspensions and scattering films. ZnO-based TCOs are especially attractive due to the lower cost and higher abundance of zinc with respect to indium and lower toxicity with respect to antimony.

In this manuscript, we report for the first time the synthesis of GZO thin films from colloidal NCs that transmit light in the visible and absorb in the NIR. Hot injection of a concentrated solution of suitable precursors into a mixture of organic amines leads to uniform NPs with narrow size distribution and tunable gallium amount. Such nanocrystals protected by organic surfactants and dispersed in proper solvents (colloidal inks) are used for the deposition of TCO coatings by spinning and

Received: August 10, 2012
Published: February 8, 2013

   dx.doi.org/10.1021/ja307960z | J. Am. Chem. Soc. 2013, 135, 3439−3448

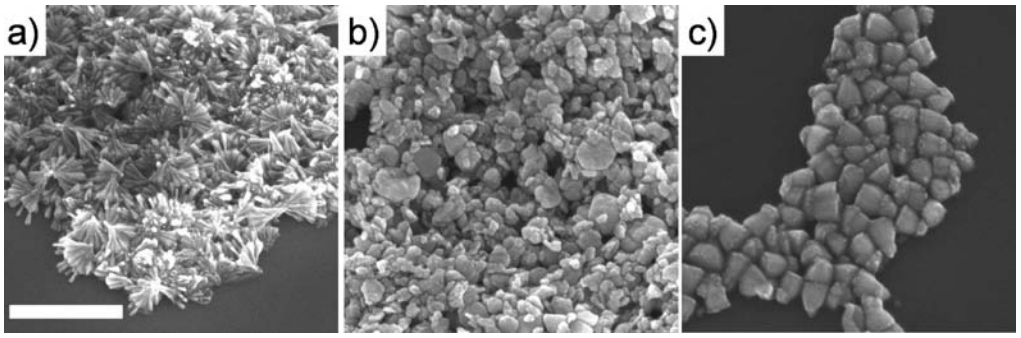

Figure 1. SEM micrographs of GZO3 NCs synthesized with different reaction conditions: (a) synthesis performed in pure TOA; (b) synthesis performed in a mixture of OA and TOA heating the reaction mixture from room temperature directly at 310 °C; (c) synthesis performed using TOP as a capping agent. The scale bar is 500 nm, and it is common to all images.

spraying. A general strategy for improving the opto-electronic properties of the coating without high-temperature treatments is also reported, resulting in high-quality films with optical and electrical performances directly comparable with ITO colloidal coatings.

2. RESULTS AND DISCUSSION

2.1. Nanocrystal Synthesis. Ga-doped ZnO NCs were synthesized by injecting a solution of the precursors (zinc stearate, $ZnSt_2$, and gallium nitrate, $Ga(NO_3)_3$) dissolved in oleylamine (OA) into a hot (310 °C) trioctylamine (TOA) solution under a nitrogen blanket, resulting in a Ga/Zn molar ratio up to 5%. After the completion of the reaction, the particles were washed with ethanol and acetone and redispersed in nonpolar solvents. The samples are labeled GZO*X* where *X* is the nominal Ga/Zn ratio in molar percent. To increase the free charge concentration, we used forming gas (95% Ar/5% H_2) treatments, performed either on the colloidal GZO solutions or on dry films.

The synthetic procedure adopted here is the result of a tailoring process starting from the approach presented by Yang and co-workers for doped ZnO nanowires:[14] in order to obtain small and spherical particles to achieve high transparency in the visible minimizing light scattering, different solvents, capping agents, precursors, injection temperatures, and heating profiles have been used. Some results of the optimization study are presented in Figure 1: for example, the synthesis performed in pure TOA (Figure 1a) leads to long rod or wire formation, often grouped in clusters or bundles arising from a common base, according to the reaction time and temperature, as observed also previously.[14] The addition of oleic acid in the reaction mixture has a similar effect, promoting as well wire formation, as also shown in other publications.[15]

Without performing the injection of the precursors at high temperature but simply heating the mixture from room temperature directly at the reaction temperature, bigger particles with greater size distribution are formed (Figure 1b). Other capping agents have been proven ineffective to reduce the particles size: for example, by using trioctylphosphine (TOP), rather isotropic and faceted NPs with a slight truncated pyramid shape but with size in the 50−100 nm range are formed (Figure 1c). All these syntheses resulted in crystalline materials, with only wurtzite−ZnO diffraction peaks detected in the X-ray diffraction (XRD) patterns.

For the optimized conditions (see the Experimental Section for details), as-synthesized GZO NPs are crystalline as well, and the XRD data showed only ZnO-related peaks (Figure 2a)

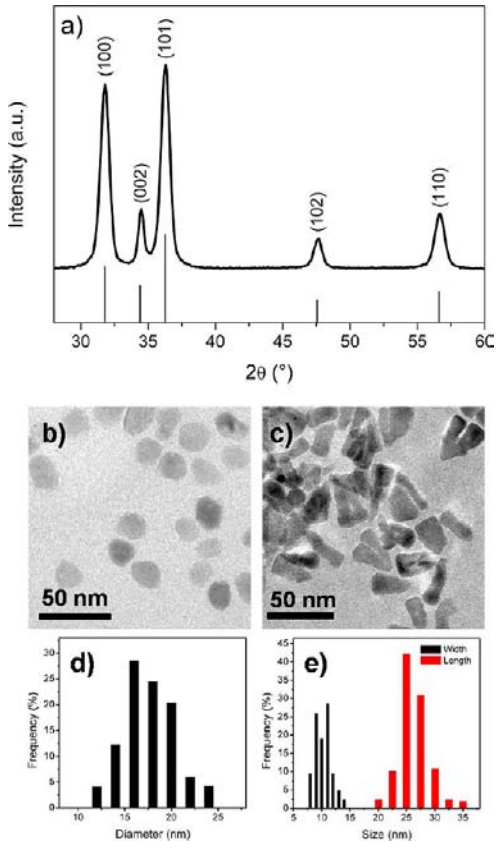

Figure 2. (a) XRD pattern of a typical Ga−ZnO sample; theoretical diffraction peaks position for wurtzite−ZnO are shown as vertical lines. TEM images of (b) pure ZnO and (c) GZO3 NCs. Size distribution histograms for (d) ZnO and (e) GZO3 are also reported.

assigned to the hexagonal wurtzite structure (JCPDS no. 36-1451). No significant variation in XRD peaks has been detected among the different samples in this study, but a slight variation in their relative intensity and broadening can be observed (Figure S1, Supporting Information). These effects are assigned to variations in the shape and size of the nanocrystals due to the presence of dopant ions in the growth solution and not to changes in the crystal structure or strain. In detail, a steady increase in the crystallite size along with Ga doping is observed for the peak corresponding to the (002) diffraction, that is, the direction along the *c* axis of the hexagonal cell, whereas the general trend with increasing the dopant concentration is a slight broadening of the diffraction peaks, resulting in a smaller

dx.doi.org/10.1021/ja307960z | *J. Am. Chem. Soc.* 2013, 135, 3439−3448

crystallite size, that reaches a minimum for a dopant concentration between 3% and 4% (Table S1, Supporting Information). This is ascribed to a certain degree of anisotropy in the shape of the particles caused by the presence of $Ga(NO_3)_3$, as will be clarified along with electron microscopy characterization. It is worth pointing out that the substitution of Zn^{2+} with Ga^{3+}, a slightly smaller ion, should lead to a shift of the diffraction peaks toward greater angles, due to the reduction in size of the crystal cell. Wang et al. observed an opposite trend for GZO powders sintered at high temperature, as a consequence of the slightly increased distance of Zn−O and Ga−O bonds at high free electron concentrations.[16] Interstitial Ga^{3+} ions might be a cause of an increase in the crystalline cell volume as well, even if their presence is energetically unfavorable. Thus, it is likely that a combination of these contributions is responsible for the negligible shift we observed in the samples prepared in this study.

The chemical composition of the colloids has been monitored using inductively coupled plasma mass spectrometry (ICP-MS) after dissolving the GZO powders in concentrated acids as described in the Experimental Section: increasing the amount of Ga precursor introduced in the synthesis causes an increase in the Ga doping, as expected (Table S2, Supporting Information). The deviation from the nominal value observed is in agreement with already published results for ITO[9] and AZO[12] where the experimental dopant concentration as measured with ICP was lower than the nominal value, especially for larger dopant amounts.

Transmission electron microscopy (TEM) analyses show the presence of rather spherical nanoparticles for pure ZnO as well as for low Ga concentration, but slightly elongated for higher Ga concentration, confirming the influence of the dopant salt in the NC shape (Figure 2b,c). The ZnO NC size distribution is rather narrow, with an average size of 17.6 ± 2.3 nm (Figure 2d); at high Ga concentration, the NCs become anisotropic, but the size is still relatively small: for example, GZO3 NCs have an average length of 26.2 ± 2.4 nm and an average width of 10.31 ± 1.9 nm, as shown in Figure 2e. In both cases, actual nanoparticle size agrees with size estimates from XRD peak-broadening (Scherrer analysis).

The effect of dopant ions in the structural properties of ZnO colloids has been investigated recently, confirming their active role in defining the size and shape of the synthesized NCs.[17,18] To investigate the effect of the gallium precursor, we performed a synthesis of undoped ZnO NCs, using a mixture of 97% $ZnSt_2$ and 3% zinc nitrate, $Zn(NO_3)_2$: we did not see any appreciable difference in size and shape in comparison with the ZnO NCs synthesized starting from pure $ZnSt_2$, suggesting a role of Ga^{3+} rather than NO_3^- in affecting the shape of ZnO colloids. The $Ga(NO_3)_3$ effect in promoting the elongated shape of ZnO NCs has been observed also in the past, where more uniform GZO nanowires could be obtained with respect to AZO and undoped ZnO ones.[15]

Optical absorption spectra of the doped colloids (Figure 3) show a clear absorption feature starting at a wavelength of ∼1200 nm, while the colloidal solutions retain a reasonable transparency in the visible range. This effect is due to the increase in free electron density provided by the Ga^{3+} ions substituting the Zn^{2+} ions: as a matter of fact, GZO NCs are nanoparticles with a surface plasmon resonance peak in the IR region. The rise in absorbance observed in the NIR is the onset of the surface plasmon resonance peak.[9] Moreover, the strong UV absorption edge typical of ZnO is registered at about 380

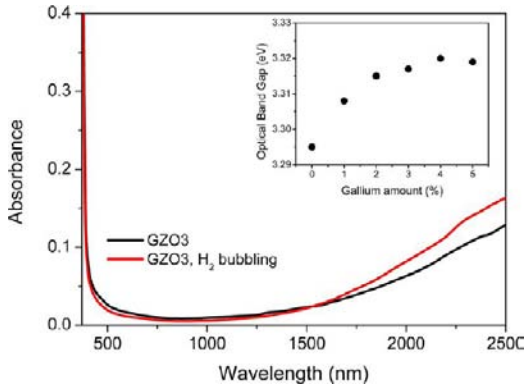

Figure 3. Optical absorption spectra in the UV−visible−NIR range for GZO3 colloids with (red line) and without (black line) the hydrogen bubbling treatment, illustrating their transparency in the visible and strong IR absorptions. The inset shows the optical band gap evaluated from the absorption spectra as a function of the gallium amount.

nm, and it is found to slightly blueshift with increasing Ga concentration, as shown in the inset of Figure 3. Given that the NCs synthesized in this study are 15−25 nm in size and that the ZnO electronic properties are size-dependent only at particle sizes below 7−10 nm,[19] the observed blueshift (i.e., increase of the optical band gap) is ascribed to the increased electronic density as a consequence of the Ga doping (the Burnstein−Moss effect) and not to quantum size effects.

A small increase in the IR absorption is observed in the hydrogen-treated colloids (red line in Figure 3), indicating an increase in the number of charge carriers provided by exposure to a reducing atmosphere. In some samples, we noticed also a slight improvement in the transparency in the visible range after the hydrogen bubbling treatment, possibly as a consequence of the improved dispersibility: in fact, by creating oxygen vacancies, the surface of ZnO crystals becomes richer in cations, that can be easily coordinated by the amines used as solvents, improving the colloidal dispersion.[20] It is worth underlining that the effect of hydrogen exposure on the optical and electrical properties of ZnO is not entirely clear. In fact, besides the possible increase in oxygen vacancies concentration, the presence of hydrogen multicenter bonds has been also hypothesized: as described by Janotti and Van De Walle, hydrogen can substitute oxygen in metal oxides such as ZnO, becoming 4-fold coordinated with unexpected bond stability, thereby explaining the observed n-type behavior of undoped ZnO and the conductivity dependence on oxygen partial pressure.[21]

2.2. Thin Film Deposition. *2.2.1. Optical and Morphological Characterizations.* As discussed in the Introduction, these colloidal solutions are used to deposit nanocrystalline GZO thin films at low temperature. The prepared colloids were thus dispersed in toluene and deposited on glass or silicon substrates by spin coating. High-quality, uniform, and homogeneous coatings over several micrometers can be observed in scanning electron microscopy (SEM) micrographs (Figure 4a−d), without any crack formation or wetting/adhesion problems. In addition, the effect of the gallium concentration in the NCs size and shape discussed previously can also be easily seen in the high-resolution images (Figure 4e−h). SEM investigation on samples that underwent the different treatments described in the Experimental Section (forming gas exposure of both colloidal solutions and dry films)

dx.doi.org/10.1021/ja307960z | J. Am. Chem. Soc. 2013, 135, 3439−3448

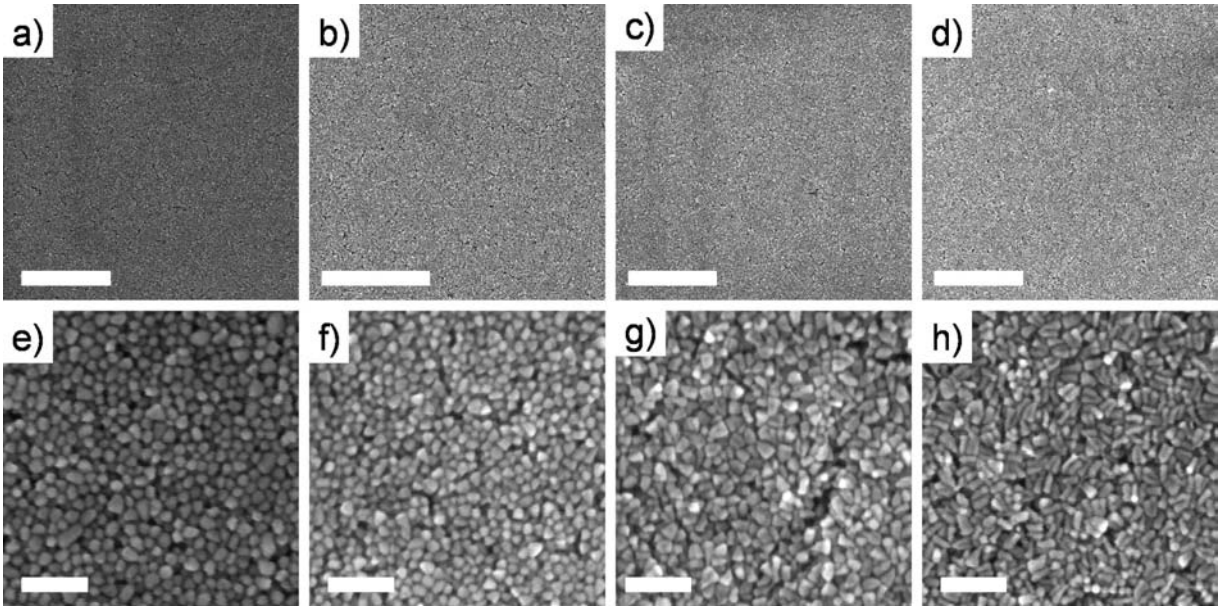

Figure 4. SEM micrographs at different magnifications of Ga-doped ZnO films with different Ga amounts: (a, e) 0%; (b, f) 1%; (c, g) 2%; (d, h) 3%. The scale bars are 1 μm for images a–d and 100 nm for images e–h. The good uniformity of the films over several micrometers as well as the steady change in shape of the NCs from spherical and isotropic to conical and elongated with increasing Ga amount can be observed.

reveals that these processes do not affect the crystals size or shape, as reported in Table S1 and Figure S2 in the Supporting Information.

To probe the chemical composition and the relative amount between Ga and Zn among the deposited samples, energy-dispersive X-ray (EDX) compositional analysis and Auger electron spectroscopy (AES) were employed (Figures S3 and S4, Supporting Information). The average chemical composition of the different samples reflects fairly well the nominal one and the results obtained from ICP analysis on the GZO powders as well, with a progressive increase in the detected gallium signal with increasing the amount of the Ga precursor introduced in the NCs synthesis solution, even if the measured content of Ga is lower than the nominal one. Since the energies associated with Ga and Zn signals in the EDX scans are very close and the amout of Ga is small with respect of Zn, the error associated with the EDX evaluation is fairly large, but nonetheless, a clear trend can be observed.

Interestingly, the composition obtained by AES is different than the nominal values in the growth solution: the Ga amount is about 10% in the 5% nominal sample. A dopant amount slightly higher than expected has been also found in the other samples. Since the escape depth of Auger electrons is small (2–3 nm), the results seem to indicate a dopant segregation at the surface of the particles. This may point to a thermally induced diffusion of the dopants toward the surface,[22] or as observed recently for AZO colloids,[12] the dopants may be excluded from the initial nuclei, and then, their incorporation rate increases with reaction time, resulting in a greater concentration at the surface of the NCs.

In order to explore the industrial applicability of the developed colloids, GZO thin films have been deposited also by spray coating. To avoid the use of hazardous chemicals, we transferred the GZO nanocrystals from nonpolar solvents to ethanol, replacing the native ligands with a new capping agent, 5-amino1-pentanol (APOH), as described in the Experimental Section. Thanks to its polar end, APOH makes the colloids easily dispersible in polar solvents such as alcohols. Spray-coated films were extremely uniform and homogeneous over several tens of micrometers, as reported in Figure 5a confirming the direct applicability of these materials for coating of wide areas with a simple and cheap technique.

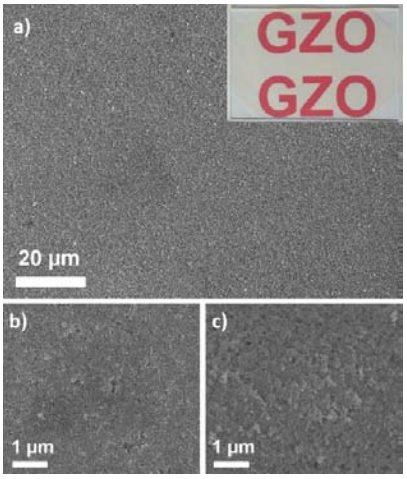

Figure 5. (a) SEM micrograph of a GZO3 film deposited by spray coating, showing the uniformity and homogeneity of the coating (the area is about 10 000 μm^2). The inset shows a picture of a glass slide covered with about 1.5 μm thick GZO3 coating, highlighting the good optical quality of the deposited film. The size of the coated glass slide is 5 cm × 7.5 cm. (b) SEM micrograph of a GZO3 film spin coated from a dispersion of NCs in toluene. (c) SEM micrograph of a GZO3 film spin coated from a dispersion of NCs in ethanol.

Some samples have been spin coated from ethanolic solutions as well and compared with films deposited by spinning the nanocrystals dispersed in toluene: similar morphologies between the two sets of samples have been observed with SEM (Figure 5b,c), suggesting that both the ligand exchange procedure and the solvent used for the depositions do not play a relevant role in the sample

dx.doi.org/10.1021/ja307960z | J. Am. Chem. Soc. 2013, 135, 3439–3448

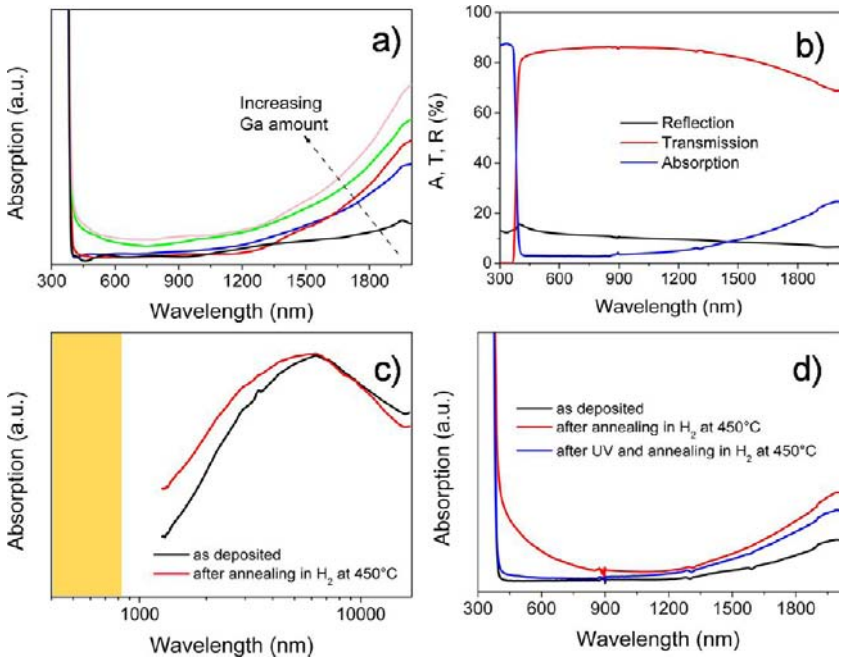

Figure 6. (a) Optical absorption spectra of GZO films with different Ga amounts. (b) Optical absorption (A), transmission (T), and reflection (R) spectra for a GZO2 film. (c) FTIR spectra of a GZO3 film as deposited (black line) and after the annealing in 95% Ar/5% H_2 atmosphere at 450 °C (red line); the orange box highlights the visible range. (d) Optical absorption spectra for a GZO3 film as deposited (black line), after the annealing in 95% Ar/5% H_2 atmosphere at 450 °C (red line) and after the same annealing and the UV treatment (blue line).

morphology and properties. Moreover, similar sheet resistance values have been measured on samples with similar thickness and the same Ga amount deposited from ethanol and toluene solutions that underwent the same postdeposition treatments (UV exposure and annealing in forming gas).

Optical characterization of GZO films is presented in Figure 6: the optical properties of the colloidal solutions are retained in the films as well, with both the distinctive absorptions in the near UV and the NIR and the transparency in the visible. A progressive increase in the IR absorption along with the Ga amount is observed, even if for high Ga doping the transparency in the visible is slightly reduced (Figure 6a): this is consistent with the increased electron concentration provided by a greater gallium doping, as reported previously also for other colloidal TCOs nanocrystalline coatings.[9,12] Figure 6b shows the optical absorption, transmission, and reflection spectra of a GZO2 film deposited on silica glass substrate: we observed optical transmission in the visible range greater than 85%, while absorption is negligible and the remaining 10−15% is due to reflection. In fact, ∼8% of the reflection is due to the glass substrate, and the remaining reflection is due to the high refractive index of the GZO coating (see below). With this considered, the transmission of the GZO film itself greatly exceeds 90%, being comparable with the properties obtained for GZO[23] and even other TCOs (namely, AZO[24] and ITO[25]) dense coatings deposited with well-established physical techniques. Again, the NIR absorption due to the free charge carriers is clearly observed.

As anticipated before, the absorption in the NIR is the onset of the plasmon resonance arising from the free carriers provided by Ga doping: Fourier transform IR (FTIR) spectra of a GZO3 sample deposited on silicon substrate (Figure 6c) show the broad surface plasmon resonance peak centered around 6 μm, and interestingly, the peak is shifted at shorter wavelengths after the annealing in reducing atmosphere, suggesting an increase in the amount of free carriers. In fact, as described by Mie theory,[26] the surface plasmon resonance frequency is proportional to the square root of the free electron concentration, and an increase in the electron amount causes an increase in the surface plasmon resonance frequency, consistent with the observed blueshift.

We analyzed in detail the effect of thermal annealing under reducing atmosphere: while it is known that a thermal treatment in air causes a decrease of the IR absorption of TCO films as a consequence of the decrease in oxygen vacancies concentration,[27,28] annealing performed under reducing gases is a useful strategy to improve the performances of TCOs.[29] The optical absorption spectra of a GZO3 film as deposited (black line) and after the annealing procedure in reducing atmosphere (red line) are shown in Figure 6d. The IR absorption is clearly enhanced, as a consequence of the previously described blueshift of the surface plasmon resonance frequency, but the transparency in the visible range is somewhat compromised. The reduced visible transparency is due to residual carbon species resulting from amine decomposition during the heat treatment. As a matter of fact, the samples have a pale yellow-orange color after the annealing. To avoid this effect, the organic compounds were first decomposed by UV light, exploiting the photocatalytic properties of ZnO.[30,31] With a simple exposure to UV light in air at room temperature, the organic molecules (essentially amines that act as capping agents for GZO colloids) can be decomposed, and this process can be easily monitored with FTIR (Figure S5, Supporting Information). The last spectrum reported in Figure 6d (blue line) refers to the same GZO3 film annealed under a reducing atmosphere following a 45 min exposure to UV radiation. The coating retained the transparency in the visible range, while displaying increased IR absorption compared to the as-deposited film. This UV treatment does not affect the nanoparticles

dx.doi.org/10.1021/ja307960z | J. Am. Chem. Soc. 2013, 135, 3439−3448

morphology, and it is useful also to improve the conductivity of the nanocrystalline films, as will be discussed below.

The UV light exposure has two effects: removal of the organic compounds and removal of adsorbed oxygen species, which act as electron traps.[32,33] While the first effect is permanent, the second is completely reversible as soon as the UV source is removed and oxygen is restored in the environment. To analyze these effects, we combined two experiments: first, we collected the optical spectra of a GZO film before and after the UV exposure performed in air under ambient conditions. As expected, the UV treatment does not affect the IR absorption properties as shown in Figure 7a,

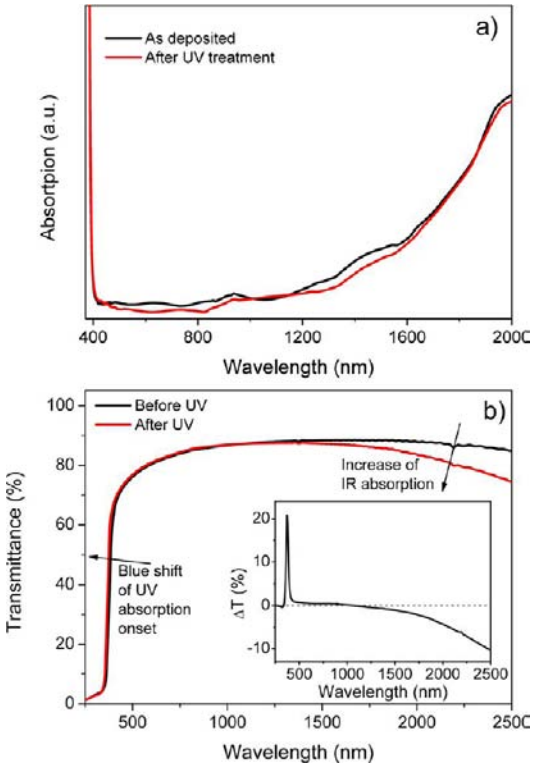

Figure 7. (a) Optical absorption spectra of a GZO2 thin film as deposited (black line) and after 45 min of UV light exposure in air (red line). The figure highlights the negligible effect of the UV treatment performed in air on the optical properties of the Ga-doped ZnO films. (b) Optical absorption spectra of a GZO1 film under N_2 atmosphere before and after exposure to UV light. The UV exposure causes a blueshift of ZnO band gap and an increase of IR absorption. The inset shows the variation in transmittance (ΔT), defined as the difference between the spectrum after UV exposure and the spectrum before UV exposure: the effect on the band gap and the IR absorption is evident.

because the number of free electrons remains unchanged. The second experiment was carried out exposing a thin sample with low Ga doping, chosen to show a weak IR absorption as a consequence of the low free electron concentrations and the presence of electron traps, to UV light keeping it under a nitrogen stream in a closed cell provided with gas inlet and outlet and pure silica windows. UV−visible−NIR spectroscopy was performed: after turning off the UV lamp while still keeping the sample under a nitrogen stream, we observed a blueshift of the optical band gap (Burnstein−Moss effect) and an increase of the IR absorption as a consequence of the greater number of free electrons generated after the oxygen traps removal (Figure 7b).

When air is let flow inside the test cell, this effect is lost in a time scale of a few tens of minutes. This experiment provides a further confirmation of the mechanism responsible for the IR absorption, that is, the increase in the number of free electrons.

GZO films have been further characterized with spectroscopic ellipsometry (Figure S6, Supporting Information). The refractive index of the coatings was found to be close to 1.65 in the visible range, much lower than the expected value for fully dense ZnO (around 2 at 600 nm).[34,35] This difference is ascribed to porosity, as evident also from SEM images, and by utilizing effective medium approximation models,[36] a pore volume fraction of ∼30% has been estimated. Moreover, the experimental Ψ and Δ values in the visible and NIR range have been fitted assuming a simple Cauchy dispersion for the refractive index of pure ZnO, but the model diverged for GZO films. In order to improve the fitting results, a Drude oscillator was added in the NIR region in order to better fit the IR absorption, as shown in the inset of Figure S6 (Supporting Information), confirming again the metal-like behavior in the IR region due to the large number of free carriers.

In order to study the sub-bandgap absorption of these materials more accurately, sensitive spectroscopic measurements were performed using photothermal deflection spectroscopy (PDS): this technique allows probing of the low-absorption states in the gap created by the different postprocessing steps described in this study. Three films of GZO5 nanocrystals were deposited onto quartz substrates: a control without any type of treatment, a second one with forming gas treatment in solution, and a third with forming gas treatment at 450 °C after film deposition. The obtained PDS spectra are reported in Figure 8: it is evident that each treatment step increases the density of tail states extending from the band edge, which is indicative of a larger concentration of near-edge defect and impurity states. The deep sub-bandgap region is also affected, with the untreated film having the lowest amount of absorption, followed by the

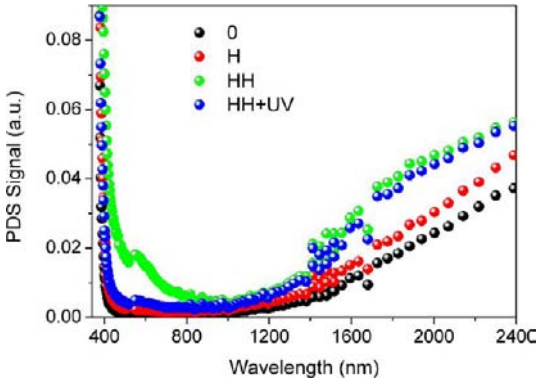

Figure 8. PDS spectra of a GZO5 film as a function of the colloids and films treatment (0 = no treatment; H = 95% Ar/5% H_2 gas bubbling in the colloidal solution; HH = film annealed in 95% Ar/5% H_2 atmosphere at 450 °C; HH+UV = film annealed in 95% Ar/5% H_2 atmosphere at 450 °C and then exposed to UV light). Both the 95% Ar/5% H_2 gas bubbling treatment and the annealing under the 95% Ar/5% H_2 atmosphere increase the IR absorption of the GZO films. Moreover, the UV light exposure helps to increase the transparency in the visible range, removing the organic compounds, avoiding the formation of residual carbon during the annealing.

dx.doi.org/10.1021/ja307960z | J. Am. Chem. Soc. 2013, 135, 3439−3448

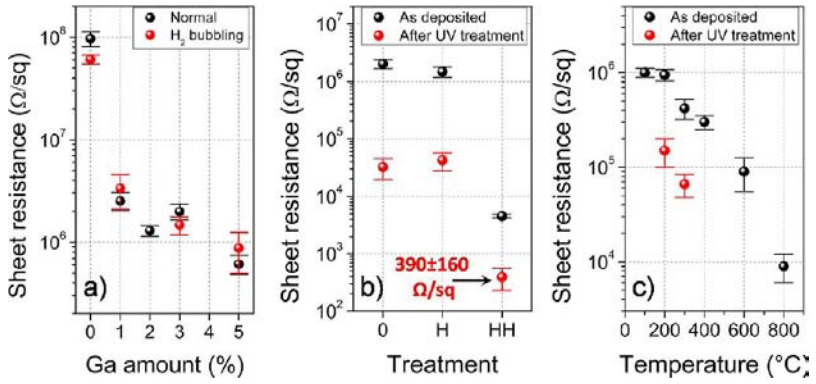

Figure 9. (a) Sheet resistance of ZnO films according to Ga amount. (b) Sheet resistance of GZO3 films according to the hydrogen treatment (0 = no hydrogen treatment; H = 95% Ar/5% H_2 gas bubbling in the colloidal solution; HH = film annealed in 95% Ar/5% H_2 atmosphere at 450 °C). (c) Sheet resistance of GZO2 films annealed in air at different temperatures.

treated-in-solution material and the film-annealed sample having the largest absorption, with the corresponding detrimental effects on transparency. Postannealing UV treatment of the film-annealed sample resulted in a decrease in both the near-band edge and deep sub-bandgap absorption, without reverting however to nontreated levels.

PDS has been previously used to assess doping efficiency in ZnO nanoparticles and is useful in this case to quantitatively study the average electrical properties of an ensemble of nanocrystals. By fitting the infrared region of the spectrum to that of a Drude metal, we obtain the average free charge density and mobility for each sample (Table S3, Supporting Information). The UV/H_2 treatments described in this work result in a significant (~30%) increase in the free charge density from 9.6×10^{19} to 12.2×10^{19} cm^{-3}, at the cost of a non-negligible decrease in the mobility from 28.7 to 24.0 $cm^2/(V\,s)$, likely due to the increased defect density.

2.2.2. Electrical Characterization. Electrical characterization has been carried out in order to understand the effects of dopants, hydrogen treatment, and postprocessing of the GZO films: all the results are reported in Figure 9. A clear decrease in sheet resistance of ~2 orders of magnitude has been observed in the doped films with respect to the undoped case (Figure 9a), as a consequence of the increased density of free carriers generated by Ga^{3+} doping. The decrease is very pronounced for low Ga concentrations, while for higher doping levels, the incremental resistance change is not as large. Previous studies on Ga- or Al-doped ZnO films deposited by sputtering,[37] sol–gel,[38] colloidal techniques,[39] microwave irradiation,[40] pulsed laser deposition,[41] and CVD[42] revealed that the electrical properties of doped ZnO samples depend on the dopant concentration but without a definite trend, since the highest conductivity can be achieved with dopant amounts between 0.5% and 6%, according to the specific synthetic procedure.

The observed increase in optical absorption in the NIR along with gallium amount is accompanied by a decrease in resistance, as expected considering the increased number of free electrons available in the ZnO conduction band. A slight decrease in optical transmittance in the visible is experienced at high gallium doping levels, but the overall transmittance remains greater than 90% as discussed previously. All these results are summarized in Figure S7 in the Supporting Information.

The hydrogen treatment of the colloids seems to have little or no effect on the conductivity (Figure 9a), since the variation of the resistance is within the error bars. This effect might be due to the previously discussed increase in dispersion of the colloids treated with hydrogen, related to a higher amount of organic molecules present at the surface of the particles. As a result, the increase in free carrier concentration caused by hydrogen is balanced by the increase in interparticle resistance. The conductivity of the as-deposited NCs assemblies is fairly high, but it can be improved by removing the organic compounds, reducing the interparticle resistance: after the previously described UV treatment, the conductivity of the films is improved by at least 1 order of magnitude (Figure 9b). The sheet resistance of UV-exposed GZO NCs assemblies without any thermal annealing besides the mild drying at 60 °C is in the 30–40 kΩ/sq range, directly comparable with the electrical performances of ITO colloidal coatings recently published,[9] even using commercially available ITO NCs.[43] Films annealed in reducing gas atmosphere at 450 °C underwent a decrease in resistivity of 2–3 orders of magnitude (Figure 9b), due to the increase in charge carrier concentration, as already reported for several TCOs films.[30] After this annealing, the sheet resistance drops down to 300–400 Ω/sq, again reaching state of the art performances of ITO colloidal coatings after annealing[10] and just 1 order of magnitude away from commercially available ITO coatings.[44]

We tested also samples with different thicknesses in order to evaluate the effect of the films thickness on their optoelectronic properties: decreasing the sample thickness causes a greater transparency in the visible range due to less scattering and less reflection, but at the same time, the absorption in the infrared is reduced as well (Figure S8, Supporting Information). As far as the electrical properties are concerned, the sheet resistance slightly increases at low thicknesses, but it remains fairly close to the values presented in Figure 9 and so still comparable to the previously published best results for ITO, as discussed before.

Moreover, similar sheet resistance values have been observed for samples deposited from ethanol after the ligand exchange process, confirming that this procedure does not affect the electrical properties of the GZO colloidal films.

Thermal annealing in air causes a slight decrease in resistance up to 400 °C; then, for higher temperatures, the decrease in resistance is much more pronounced (Figure 9c). Interestingly, annealing at 300 °C followed by the UV treatment gives about the same resistance as annealing at 600 °C. At temperatures higher than 550 °C, all the organic compounds are

dx.doi.org/10.1021/ja307960z | J. Am. Chem. Soc. 2013, 135, 3439–3448

decomposed, as confirmed by thermogravimetric (TG) analysis measurements (Figure S9, Supporting Information). This suggests that the organic ligands can be removed by UV treatment or by annealing in air, giving the same results in terms of electrical properties of the films, confirming the role played by organic compounds in lowering the conductivity by hindering interparticle charge transfer.

A control experiment has been performed on film annealed at 600 °C, where all the organic ligands are removed (as proved by FTIR). No appreciable variation in sheet resistance has been detected in such film before and after UV treatment in air, confirming that the observed decrease in sheet resistance observed after the UV exposure on the as-deposited films is due to the removal of the organic compounds and not to an electronic effect.

The developed GZO colloidal inks can thus be used to deposit at low temperature conductive coatings that are transparent in the visible range and absorb in the NIR. Depositions techniques such as spin coating and spraying has been proved effective to deposit high quality films, even on large substrates. Moreover, GZO patterns can be easily obtained by loading a NCs ink solution inside an inkjet printer allowing the deposition of low-cost active films with the desired pattern and/or shape on several different substrates. Eventually, these NCs can be mixed with polymers to obtain UV blocking, visible transparent, and IR absorbing/reflective flexible coatings. For example, GZO nanocrystals could be embedded inside films of polyvinylbutyral (PVB), the polymer used as the interlayer in car windshields. If the conductivity of the polymer−oxide composites is sufficiently high, it would enable their use also as antistatic coatings. This synthetic approach has also been found successful in preparing also AZO NCs, simply substituting the gallium precursor with aluminum stearate (Figure S10, Supporting Information).

3. CONCLUSIONS

Ga-doped ZnO NCs have been synthesized by colloidal techniques, obtaining uniform NPs with tunable composition; these surfactant-protected colloids show significant optical absorption in the UV and IR and high transparency in the visible range. The electrical properties of the NCs are successfully modified due to the substitution of Ga^{3+} ions in Zn^{2+} lattice sites. Thin films deposited from these colloidal inks are extremely homogeneous and uniform, and they retain the distinctive optical properties of the NCs solutions. Detailed microstructural, optical, and electrical characterizations have been performed to explain the effect of dopant concentrations, reducing atmosphere annealing and postprocessing of the films on their optical and electrical properties. Deposition techniques such as spin coating and spray coating have been proved to be effective to deposit low-cost and high-quality films from colloidal solutions in both polar and nonpolar solvents. Transmittance in the visible greater than 90%, tunable IR absorption, and electrical properties comparable to ITO NCs assemblies are achieved, highlighting GZO colloidal coatings as a valuable alternative to traditional TCO films.

4. EXPERIMENTAL SECTION

4.1. Nanocrystal Synthesis. All chemicals have been purchased from Aldrich and used without any further purification. All syntheses are performed with standard Schlenk line techniques. $ZnSt_2$ and $Ga(NO_3)_3$ are dissolved in 7.5 mL of OA at 80 °C (solution 1) under a nitrogen stream, keeping the atomic concentration (Zn + dopant) equal to 0.4 M and the Ga/Zn molar ratio between 0% and 5%. Separately, 22.5 mL of TOA is heated under nitrogen at 100 °C (solution 2), degassed under vacuum for 2 min, and then, heated under nitrogen at 310 °C.

Solution 1 is then degassed for 5 min and quickly injected into solution 2 at 310 °C. The temperature drop is less than 40 °C. The total solution is let stir at 280 °C for 25 min and then cooled down to room temperature. The doped ZnO NCs are precipitated with ethanol or acetone, centrifuged at 4000 rpm for 5 min, and redispersed in a variety of nonpolar solvents such as toluene, tetrachloroethylene (C_2Cl_4), hexanes, and so forth. The samples are labeled GZO*X* where *X* is the nominal Ga/Zn molar percentage. The reaction yield was found to be between 85% and 90%.

A subsequent treatment is performed in order to increase the free charge density: the NCs are dispersed in a mixture of 1-octadecene (ODE, 15 mL), TOA (0.5 mL), and OA (0.5 mL) with a nominal concentration of 0.1 M, degassed at 90 °C, and heated up to 150 °C under a nitrogen stream. Then a 5% hydrogen/95% argon mixture stream is bubbled inside the solution through a stainless steel needle for 25 min with a flow rate of approximately 0.1 L/min, and the solution is subsequently cooled down to room temperature under the reducing atmosphere. In the manuscript, we refer to this procedure as "hydrogen bubbling treatment". The NCs are then washed with acetone and redispersed again in nonpolar solvents.

If needed, GZO NCs were transferred to ethanol by exchanging the surface ligands (organic amines) with APOH: the procedure is performed by adding 5 mL of a 10 g/L APOH solution in chloroform to 7.5 mL of a 0.1 M GZO colloidal solution in C_2Cl_4 under stirring. Immediately upon addition of the APOH solution, aggregates appear, suggesting partial ligand exchange. After 30 min, the aggregates are collected by centrifugation (1000 rpm, 4 min), resuspended in 5 mL of a 0.5 g/L APOH solution in chloroform to induce further ligand exchange, stirred for an additional 15 min, centrifuged (1000 rpm, 4 min), and eventually, resuspended in ethanol to a 40 mg/mL stock solution.

4.2. Thin Film Synthesis. GZO thin films are deposited from concentrated NC solutions in toluene (between 40 and 80 mg/mL) by spin coating on either SiO_2 (HSQ300, Heraeus) or Si (⟨100⟩ oriented, p-type boron-doped, Silicon Materials) substrates at 1500 rpm for 40 s. After deposition, the samples are placed on a hot plate at 60 °C for 10 min. If needed, this procedure has been repeated to increase the sample thickness. The thickness of the samples used for optical and electrical characterization is about 500 nm, but thicker samples (up to 1 μm) are easily obtained with further spin-coating depositions or by drop casting the NC solution.

Some samples have been annealed in air between 100 and 800 °C for 1 h in a muffle furnace or in a 5% H_2/95% Ar mixture at 450 °C for 2 h in a tube furnace, in order to analyze the effect of temperature and annealing atmosphere on the electrical and optical properties.

Spray-coated samples were deposited from ethanolic suspensions of GZO NCs using a syringe pump connected to a pneumatic atomizing nozzle (Spraying Systems, 1/4JN-SUE15B) mounted over a heated XY translation stage. This setup allows precise control of process variables including gas/liquid flow rates, inlet gas (N_2) pressure, raster velocity, and substrate temperature. Optimization of process parameters was performed in separate experiments. The final GZO NC films were sprayed with 20 mL of GZO NCs in ethanol (2 g/L), with 60 °C substrate temperature and 29 psi for the inlet gas, resulting in a GZO NC density on the substrate of nominally 0.39 mg/cm^2.

4.3. Characterization Techniques. Dry powder samples of the NC colloidal solutions were characterized by XRD using a Philips PW1710 diffractometer. The analyses were performed using Cu Kα Ni-filtered radiation at 30 kV and 40 mA. The crystallite size has been evaluated with the Scherrer equation: the five diffraction peaks detected between 25° and 60° have been fitted with Lorentzian curves, and the crystallite size has been estimated using the full width at half-maximum (fwhm) of the fitting functions. Optical absorption spectra of colloidal solutions in C_2Cl_4 (a nonpolar solvent that does not show any intense absorption peaks in the NIR region up to a wavelength of 2.5 μm), and films were measured in the 250−2500 nm range using a

Jasco V-570 spectrophotometer. The optical band gap has been evaluated from the absorption spectra plotting the square of the absorption coefficient (α) versus the photon energy ($h\nu$) and extrapolating the results for $\alpha = 0$, as described previously.[45] TEM measurements of the oxide NCs deposited on a carbon-coated copper grid were taken with a FEI Tecnai G2 X20 X-TWIN TEM.

The concentration of gallium and zinc in the GZO powders has been determined by ICP-MS equipped with DRC for the reduction of polyatomic interferences, after dissolving the oxide powders with nitric acid and hydrogen peroxide.

The surface structure of the oxide films and their chemical composition were investigated with a FEI XL30 Sirion scanning electron microscope, equipped with an EDX spectrometer for compositional analysis. Ellipsometry quantities Ψ and Δ were measured using a J.A. Woollam V-VASE spectroscopic ellipsometer in a vertical configuration, at three different angles of incidence (65°, 70°, and 75°) in the wavelength range 300−1700 nm. Values for the real and imaginary parts of the refractive index (n and k) and film thickness were evaluated from Ψ and Δ data using the WVASE32 ellipsometry data analysis software. The data were fitted with Cauchy dispersion, Tauc−Lorentz and Drude oscillators in the nonabsorbing region, UV absorption, and IR absorption, respectively. FTIR measurements on samples deposited on Si substrates have been performed using a Jasco FT/IR-620 instrument, with a resolution of 4 cm^{-1}, averaging over 64 scans. Differential thermal analysis and thermal gravimetry analysis (DTA-TG) were performed under air flux using a Netzsch STA 409/429 instrument with a heating rate of 10 °C/min up to 1000 °C. The 4 point probe sheet resistances of thin films were measured with a Keithley 2612 as both current source and voltmeter at room temperature under ambient conditions: the final values were averaged over a minimum of five measurements for each sample.

For sensitive optical absorption measurements using PDS, thin films of GZO NCs were deposited from solution onto quartz substrates. A set of three films were studied: an untreated control, a film deposited from NCs treated with reducing gas in solution, and a film of NCs annealed in reducing atmosphere after deposition. The annealed sample was also UV treated after a first round of PDS measurements, and subsequent measurements were taken on the same spot of the film. Each film was submerged in a cuvette filled with Flourinert (3M) and aligned at the intersection of the pump and probe beams. The pump is a monochromated chopped beam from a xenon arc bulb, and the probe is a low power He/Ne laser. The pump beam is divided with a 95/5 CaF_2 beamsplitter to normalize the PDS signal and account for variations in the lamp intensity. The pump beam grazes the sample and is deflected away from it due to the change in temperature of the deflection liquid caused by the nonradiative recombination of photoexcitations in the sample. The deflection is measured by a position-sensitive photodetector, and the signal-to-noise ratio is improved by using a lock-in technique. Several spectra were recorded for each sample to ensure repeatability and lack of sample damage.

Films deposited on the Si substrate were analyzed using a PHI 700 (Ultravac-Phi) scanning Auger nanoprobe using an accelerating voltage of 20 kV and a beam current of 1 nA, with a spot size of 8−10 nm. Several spots on each sample were surveyed to check for uniformity, followed by a prolonged scan at a single location in order to improve the signal-to-noise ratio of the Auger spectra. Intensities for the main Auger peaks of the elements present in the sample (C, O, Zn, and Ga) were corrected for sensitivity, and their relative concentrations were obtained.

■ ASSOCIATED CONTENT

Supporting Information

XRD patterns, SEM micrographs, Ga concentrations evaluated from SEM-EDX analyses, AES spectra, FTIR spectra, refractive index and extinction coefficient dispersion curves, comparison between sheet resistance and optical properties of as-deposited GZO films with different Ga amounts, optical absorption spectra and sheet resistance values of GZO3 samples with different thicknesses, DTA-TG curves, characterizations of some AZO samples, and tables of crystallite size evaluated with the Scherrer formula, Ga/Zn atomic percent, and values for the free charge density and mobility for an ensemble of nanocrystals. This material is available free of charge via the Internet at http://pubs.acs.org.

■ AUTHOR INFORMATION

Corresponding Author

alex.martucci@unipd.it

Present Address

[⊥]Materials Science and Engineering, CSIRO, Bayview Avenue, Clayton, Victoria, 3168, Australia.

Notes

The authors declare no competing financial interest.

■ ACKNOWLEDGMENTS

This work was done in the framework of collaborative research activities of Technical Committee 16 (on Nanostructured Glasses), of the International Commission on Glass (ICG). S.M., R.N., and A.S. kindly acknowledge support from the Global Climate energy Project at Stanford University. Partial support by the Center for Advanced Molecular Photovoltaics (award no. KUS-C1-015-21), made by King Abdullah University of Science and Technology (KAUST), is acknowledged as well. Diane Wu is acknowledged for TEM microscopy.

■ REFERENCES

(1) Ginley, D. S.; Hosono, H.; Paine, D. C. *Handbook of Transparent Conductors*; Springer: New York, 2010.

(2) Minami, T. *Semicond. Sci. Technol.* **2005**, *20*, S35−S44.

(3) Lewis, B. G.; Paine, D. C. *MRS Bull.* **2000**, *25*, 22−27.

(4) Puetz, J.; Aegerter, M. A. *J. Soc. Inf. Display* **2005**, *13*, 321−328.

(5) Yu, Z.; Zhang, Q.; Li, L.; Chen, Q.; Niu, X.; Liu, J.; Pei, Q. *Adv. Mater.* **2011**, *23*, 664−668.

(6) Morfa, A. J.; Beane, G.; Mashford, B.; Singh, B.; Della Gaspera, E.; Martucci, A.; Mulvaney, P. *J. Phys. Chem. C* **2010**, *114*, 19815−19821.

(7) Zhou, Y.; Hu, L.; Grüner, G. *Appl. Phys. Lett.* **2006**, *88*, 123109.

(8) Puetz, J.; Al-Dahoudi, N.; Aegerter, M. A. *Adv. Eng. Mater.* **2004**, *6*, 733−737.

(9) Garcia, G.; Buonsanti, R.; Runnerstrom, E. L.; Mendelsberg, R. J.; Llordes, A.; Anders, A.; Richardson, T. J.; Milliron, D. J. *Nano Lett.* **2011**, *11* (10), 4415−4420.

(10) Lee, J.; Lee, S.; Li, G.; Petruska, M. A.; Paine, D. C.; Sun, S. *J. Am. Chem. Soc.* **2012**, *134*, 13410−13414.

(11) Muller, V.; Rasp, M.; Stefanic, G.; Ba, J.; Gunther, S.; Rathousky, J.; Niederberger, M.; Fattakhova-Rohlfing, D. *Chem. Mater.* **2009**, *21*, 5229−5236.

(12) Buonsanti, R.; Llordes, A.; Aloni, S.; Helms, B. A.; Milliron, D. J. *Nano Lett.* **2011**, *11*, 4706−4710.

(13) Wei, H.; Li, M.; Ye, Z.; Yang, Z.; Zhang, Y. *Mater. Lett.* **2011**, *65*, 427−429.

(14) Yuhas, B. D.; Zitoun, D. O.; Pauzauskie, P. J.; He, R.; Yang, P. *Angew. Chem., Int. Ed.* **2006**, *45*, 420−423.

(15) Goris, L.; Noriega, R.; Donovan, M.; Jokisaari, J.; Kusinski, G.; Salleo, A. *J. Electron. Mater.* **2009**, *38*, 586−595.

(16) Wang, R.; Sleight, A. W.; Cleary, D. *Chem. Mater.* **1996**, *8*, 433−439.

(17) Clavel, G.; Willinger, M. G.; Zitoun, D.; Pinna, N. *Adv. Funct. Mater.* **2007**, *17*, 3159−3169.

(18) Yang, Y.; Jin, Y.; He, H.; Wang, Q.; Tu, Y.; Lu, H.; Ye, Z. *J. Am. Chem. Soc.* **2010**, *132*, 13381−13394.

(19) Wood, A.; Giersig, M.; Hilgendorff, M.; Vilas-Campos, A.; Liz-Marzan, L. M.; Mulvaney, P. *Aust. J. Chem.* **2003**, *56*, 1051−1057.

(20) Cotton, F. A.; Wilkinson, G. *Advanced Inorganic Chemistry*, 3rd ed.; John Wiley and Sons: New York, 1972; pp 514−515.
(21) Janotti, A.; Van De Walle, C. G. *Nat. Mater.* **2007**, *6*, 44−47.
(22) Dalpian, G. M.; Chelikowsky, J. R. *Phys. Rev. Lett.* **2006**, *96*, 226802.
(23) Assuncao, V.; Fortunato, E.; Marques, A.; Aguas, H.; Ferreira, I.; Costa, M. E. V.; Martins, R. *Thin Solid Films* **2003**, *427*, 401−405.
(24) Kim, K. H.; Park, K. C.; Ma, D. Y. *J. Appl. Phys.* **1997**, *81*, 7764−7772.
(25) Sittinger, V.; Ruske, F.; Werner, W.; Jacobs, C.; Szyszka, B.; Christie, D. J. *Thin Solid Films* **2008**, *516*, 5847−5859.
(26) Mulvaney, P.; Liz-Marzan, L. M.; Giersig, M.; Ung, T. *J. Mater. Chem.* **2000**, *10*, 1259−1270.
(27) Yamada, N.; Yasui, I.; Shigesato, Y.; Li, H.; Ujihira, Y.; Nomura, K. *Jpn. J. Appl. Phys.* **2000**, *39*, 4158−4163.
(28) Ma, Q. B.; Ye, Z. Z.; He, H. P.; Zhu, L. P.; Huang, J. Y.; Zhang, Y. Z.; Zhao, B. H. *Scr. Mater.* **2008**, *58*, 21−24.
(29) Freeman, A. J.; Poeppelmeier, K. R.; Mason, T. O.; Chang, R. P. H.; Marks, T. J. *MRS Bull.* **2000**, *25*, 45−51.
(30) Lizama, C.; Freer, J.; Baeza, J.; Mansilla, H. D. *Catal. Today* **2002**, *76*, 235−246.
(31) Jang, E. S.; Won, J. H.; Hwang, S. J.; Choy, J. H. *Adv. Mater.* **2006**, *18*, 3309−3312.
(32) Melnick, D. A. *J. Chem. Phys.* **1957**, *26*, 1136−1146.
(33) Tanaka, K.; Blyholder, G. *J. Phys. Chem.* **1972**, *76*, 3184−3187.
(34) Bond, W. L. *J. Appl. Phys.* **1965**, *36*, 1674.
(35) Lide, D. R. *CRC Handbook of Chemistry and Physic*, 87th ed.; Taylor and Francis: Boca Raton, FL, 2007; p 10−248.
(36) Bruggeman, D. A. G. *Ann. Phys. (Leipzig, Germany)* **1935**, *24*, 636.
(37) Ma, Q. B.; Ye, Z. Z.; He, H. P.; Luo, Y.; Zhu, L. P.; Huang, J. Y.; Zhang, Y. Z.; Zhao, B. H. *ChemPhysChem* **2008**, *9*, 529−532.
(38) Lin, K. M.; Chen, Y. Y. *J. Sol−Gel Sci. Technol.* **2009**, *51*, 215−221.
(39) Lu, Z.; Zhou, J.; Wang, A.; Wang, N.; Yang, X. *J. Mater. Chem.* **2011**, *21*, 4161−4167.
(40) Jood, P.; Mehta, R. J.; Zhang, Y.; Peleckis, G.; Wang, X.; Siegel, R. W.; Borca-Tasciuc, T.; Dou, S. X.; Ramanath, G. *Nano Lett.* **2011**, *11*, 4337−4342.
(41) Singh, A. V.; Mehra, R. M.; Yoshida, A.; Wakahara, A. *J. Appl. Phys.* **2004**, *95*, 3640−3643.
(42) Zhao, J. L.; Sun, X. W.; Ryu, H.; Moon, Y. B. *Opt. Mater.* **2011**, *33*, 768−772.
(43) Chung, C. H.; Song, T. B.; Bob, B.; Zhu, R.; Duan, H. S.; Yang, Y. *Adv. Mater.* **2012**, *24*, 5499−5504.
(44) See, for example, indium tin oxide coated glass slide, Sigma−Aldrich, cat. no. 703192.
(45) Kava, L.; Stoto, T.; Gratzel, M.; Fitzmaurice, D.; Shklover, V. *J. Phys. Chem.* **1993**, *97*, 9493−9498.

■ NOTE ADDED AFTER ASAP PUBLICATION

The first authors name was incorrect in the version published ASAP February 21, 2013; it was corrected and reposted February 22, 2013.